Compact SIW-based Feeding Network for S-band Monopulse Antenna

Shita Herfiah
Radio Telecommunication and Microwave Laboratory
School of Electrical Engineering and Informatics
Institut Teknologi Bandung
Bandung, Indonesia
23220080@std.stei.itb.ac.id

Achmad Munir
Radio Telecommunication and Microwave Laboratory
School of Electrical Engineering and Informatics
Institut Teknologi Bandung
Bandung, Indonesia
munir@ieee.org

***Abstract*—One of the key components in tracking system is the antenna. Monopulse antennas frequently used in tracking system provide high accuracy and efficiency in determining the range and position of the target due to the utilization of two beams, namely, sum and difference. A hybrid junction is one type of four-port network coupler widely applied in feeding networks for providing sum and diff channels. This paper deals with the development of substrate integrated waveguide (SIW) based feeding network for S-band monopulse antenna. The use of SIW aims to overcome the bulky structure of the conventional metallic waveguide and the complex integration in a finite space. The proposed SIW-based feeding network which operates at S-band frequency is implemented using a 1.524 mm thin Rogers RO-4003C dielectric substrate. The characterization result shows that the SIW-based feeding network can achieve less than –10 dB isolation, with insertion loss about –3.99 dB, return loss less than –10 dB, and phase difference around 180°. The close match between the results enables the proposed SIW-based feeding network to be applied for the desired application in tracking system.**

***Index Terms*—Feeding network; magic-tee; monopulse antenna; S-band frequency; substrate integrated waveguide (SIW).**

I. Introduction

It is already known that monopulse method is an accurate and effective tracking technique widely applied in radar systems. The advantages of using monopulse method in radar system include high accuracy, high speed, and precise target estimation with a single pulse [1]. One of the critical components in a monopulse method is the antenna. In addition to monopulse antenna, there are several types of antennas that can be used in tracking systems as well as for communication systems which have been reported [2]–[4]. The conventional monopulse antenna such as lens antennas, slotted waveguide arrays, and parabolic antennas are usually complex, bulky, and expensive to manufacture [5]. In [6], an SIW-based antenna was used in monopulse application to achieve low antenna profile and low fabrication cost.

Typically a monopulse antenna consists of two components, namely a radiation component and monopulse network which includes a feeding network and monopulse comparator [7]. The monopulse antenna utilizes sum and diff channels to determine the distance and position of a target. Components of monopulse antenna such as radiating elements, feed networks, and monopulse comparators were primarily specifying the size and compactness of the monopulse system [8]. Power divider and directional coupler are components commonly used to provide feeding network and monopulse comparator. A 180° hybrid junctions is one type of couplers which can provide sum and diff channels. It can be implemented in many types, such as tapered coupler line hybrid, ring hybrid or rat-race, and hybrid waveguide or commonly called as Magic-Tee.

Basically the Magic-Tee is a 3-dB coupler that contains of four-ports network to achieve high isolation between two input/output ports, whereby *H*-plane and *E*-plane ports are combinable. A sum port (*H*-plane arm) and a diff port (*E*-plane arm) which can be obtained on Magic-Tee permit the processing of incident signals from two input/output ports. The incident signal to the difference port equally splits the magnitude with out-of-phase of 180°. Whilst the incident signal to the sum port equally splits the magnitude with in-phase. The design of Magic-Tee can be based on various types of transmission line classified as waveguide and planar structure including SIW configuration [9].

The structure of SIW, also called as post-wall waveguide or laminated waveguide, consists of two rows of conducting cylinders which are embedded in a dielectric substrate and connecting two parallel metal plates [10]. The synthetic metallic rectangular waveguide filled with a dielectric material enables the development of SIW in a planar shape. Therefore it can be integrated with other planar transmission line such as microstrips and coplanar waveguides on the same substrate. Furthermore, SIW technology facilitates a system on the substrate to reduce the circuit size [11]. In other words, SIW technology is an alternative technique for the design with low cost, highly integrated circuits and systems.

The isolation, power balance, and phase difference between the sum and diff channels of a monopulse network can significantly impact the pattern of antenna beams. A planar Magic-Tee with an L-shaped septum has been explored to provide wide impedance bandwidth and high isolation on all ports [12]. In [13], the Magic-Tee was proposed using a combination of a septum and metallic platform as a matching junction. While in [14], the SIW Magic-Tee, which incorporates balun in the *E*-plane arm, maintains the balance of excitation and isolation between both arms. Furthermore, a SIW Magic-Tee implemented using a slot line to achieve wider bandwidth has also been investigated [15]–[18].

This paper deals with the design and characterization of compact SIW-based feeding network implementable for S-band monopulse antenna. The conventional Magic-Tee is unsuitable for compact designs due to the presence of its vertical *E*-plane arm. Therefore the proposed design feeding network will employ a horizontal *E*-plane arm placed above the *H*-plane arm with a slot for connecting both arms. The proposed design is supposed to offer low insertion loss, high isolation between the sum and diff channels, and compact size as well.

II. SIW-based Feeding Network Design

The proposed feeding network for S-band monopulse antenna is expected to have high isolation, adequate phase balance, and compact size. Fig. 1 shows the configuration of proposed feeding network using SIW method. The input ports consist of Port #1 and Port #2, known as collinear arms, while the sum and diff ports are on Port #3 and Port #4, respectively. Port #3 forms an *H*-plane arm, and Port #4 represents the *E*-plane arm. The incident signals to the diff port, i.e., Port #4, equally split the magnitude from the input ports with out-of-phase of 180°. Whilst, the incident signals to the sum port, i.e., Port #3, equally split the magnitude with in-phase.

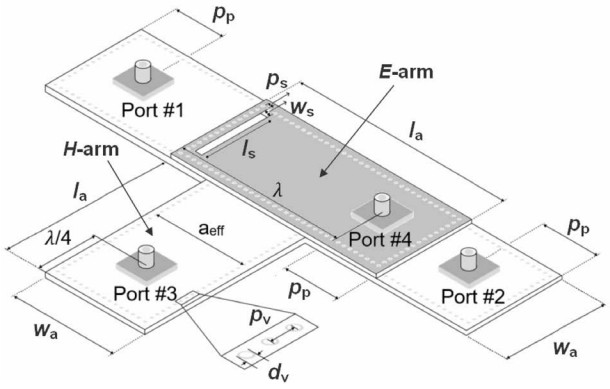

Fig. 1. Configuration of SIW-based feeding network for S-band monopulse antenna.

TABLE I
Initial dimensions of SIW-based feeding network.

Physical parameter	Symbol	Dimensions
H-arm and *E*-arm lengths	l_a	85 mm
H-arm and *E*-arm widths	w_a	43 mm
port position from wall	p_p	16.5 mm
diameter of via	d_v	1 mm
pitch of via	p_v	1.6 mm
slot position from wall	p_s	1 mm
slot widht	w_s	2.73 mm
slot length	l_s	26 mm

The proposed feeding network was designed using two layers of Rogers RO-4003C dielectric substrate with the thickness and the dielectric constants for each of 1.524 mm and 3.55, respectively. A 50 Ω SMA connector is used at all ports for excitation purposes. As illustrated in Fig. 1, all ports have the same distance to the SIW wall (p_p), i.e., $\lambda/4$. The *E*-plane arm is connected to the *H*-plane arm via a slot which is spaced 1 mm from the edge of *E*-plane arm (p_s). The length of slot (l_s) is set 0.7 times the width of *H*-plane arm (w_a). Essential parameters in the SIW design are the diameter of via (d_v), the distance between vias or pitch (p_v), and the effective width of SIW (a_{eff}) [19].

Table I shows the initial dimensions of SIW-based feeding network design following the formula in [20]. it is noted that the dominant mode, i.e., TE_{10} mode, is used for calculating the dimensions. The characterization was carried out through simulation to observe the performance of proposed SIW-based feeding network. Return loss on all ports, insertion loss, isolation, and phase difference between Port #3 and Port #4, which are the output ports, are some of performance parameters focused in the characterization. Parameter studies are also carried out to achieve good performance of the feeding network. In more detail, the impact of each dimension variation of proposed SIW-based feeding network on its performances will be described in the following subsections.

A. Variation of E-arm and H-arm Widths

The *E*-arm and *H*-arm widths are the effective SIW widths, including a 1.5 mm distance from the via edge to the edge of the *E*-arm and *H*-arm. The 1.5 mm distance for each *E*-arm and *H*-arm is a constant dimension in all characterizations and optimizations. The simulated results of return losses at the input ports, i.e., Port #1 and Port #2, and at the output ports, i.e., Port #3 and Port #4, as varied *E*-arm and *H*-arm widths are plotted in Figs. 2 and 3, respectively. It shows that the arm-width variation has an impact on the resonant frequency shifting. Based on the initial dimensions of SIW-based feeding network, the working frequencies are not at the desired one, so the optimization of *E*-arm and *H*-arm widths is necessary.

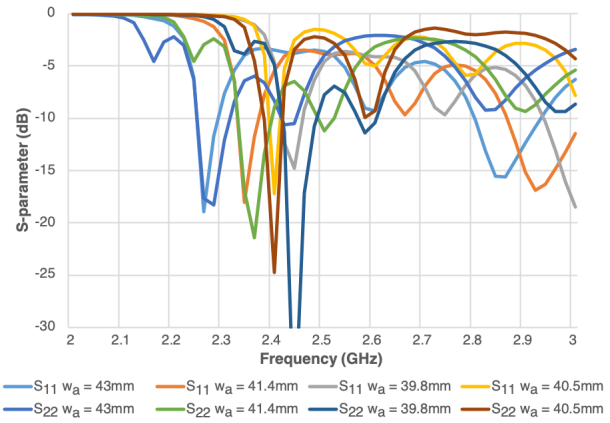

Fig. 2. Return losses at input ports as varied *E*-arm and *H*-arm widths.

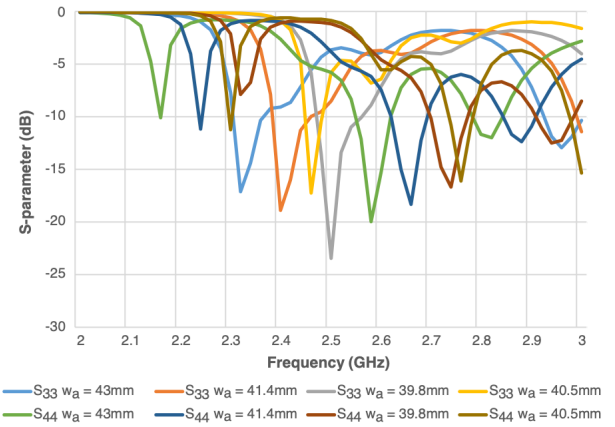

Fig. 3. Return losses at output ports as varied *E*-arm and *H*-arm widths.

Optimization is carried out either by reducing/increasing the number of via, and/or by applying the multiple of pitch. Furthermore, by using the pitch in the initial dimensions, the working frequency at the input ports is also not at the desired one, as depicted in Fig. 2. Therefore the pitch is optimized to be 1.5 mm with the *H*-arm width of 40.5 mm to achieve the desired working frequency. The diameter of via is set to be 1 mm, while the distance between vias is 1.5 mm, which is tight enough to avoid leakage on the walls of SIW.

As shown in Fig. 3, the working frequency on Port #3 and Port #4 still does not reach the desired one, so the optimization is required by reducing the *H*-arm width to be 42 mm, and the *E*-arm width to be 39 mm. However, even though the frequency on Port #3 and Port #4 has reached 2.4 GHz with the return losses of –7.691 dB and –2.712 dB, respectively, so the optimization in other dimensions is still required to obtain the return losses less than –10 dB.

B. Variation of E-arm and H-arm Lengths

The variation of *E*-arm and *H*-arm lengths is mainly to investigate the performance of SIW-based feeding network at the output ports. The simulated results of return loss at Port #4 and phase difference at the output ports are depicted in Figs. 4 and 5, respectively. It shows that the variation of arm lengths impact the depth of return loss. Based on the initial dimensions, the working frequency on Port #4 has reached the desired frequency of 2.4 GHz. However, the return loss at Port #4 requires the optimization to achieve value less than –10 dB. Here, the optimization is conducted by changing the arm lengths, whereby this will affect the number of via or the multiple of pitch. From the characterization result shown in Fig. 4, the return loss of –18.478 dB can be reached with the optimized *E*-arm length of 74.6 mm. The optimization has also an effect on the phase difference at the output ports, as plotted in Fig. 5. It can be inferred that the arm-lengths increase in proportion to the phase difference of output port.

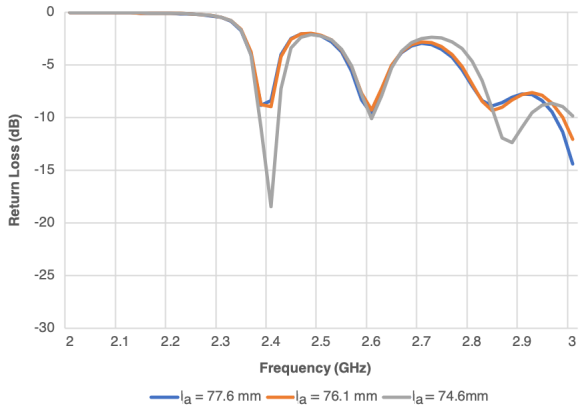

Fig. 4. Return loss at Port #4 as varied *E*-arm and *H*-arm length.

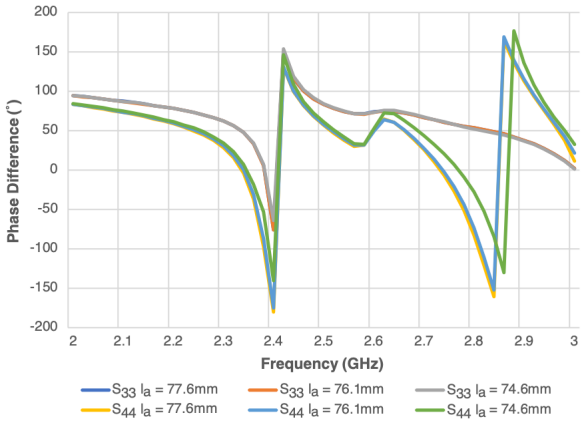

Fig. 5. Phase difference between Port #3 and Port #4.

C. Variation of Port Position

The positions of Port #3 as the critical part on the *H*-arm is initially set to be a quarter-wavelength ($\lambda/4$) from the edge of via. The simulated results for varied position of Port #3 are shown in Figs. 6 to 8. It is seen that the varied position of Port #3 affects the depth of return loss, isolation between output ports, and phase difference of output port. The position of Port #3 with the deepest return loss is at 7.3 mm as depicted in Fig. 6. It can be concluded that the closer the position of Port #3 to the edge of via, the deeper the return loss will be. The varied position of Port #3 also influences the depth of return loss at other ports, so there is a trade-off between the return loss value at Port #3 and at other ports. From the results, the 9.3 mm distance from the edge of via is to be the optimized position of Port #3.

Furthermore, the varied position of Port #3 also affects the isolation between output ports as shown in Fig. 7. In contrast to the return loss, the farther the position of Port #3 from the edge of via, the more optimal it is. It shows that the isolation of –15.287 dB can be gained by positioning Port #3 at 17.3 mm from the edge of via. The simulated result of phase difference at the output ports is depicted in Fig. 8. The farther the distance of port position from the edge of via, the more significant the phase difference obtained. The result shows a significant change, which is around 100° in all optimization processes. Moreover, the variation of Port #4 position is also carried out with the same procedure as of Port #3 position.

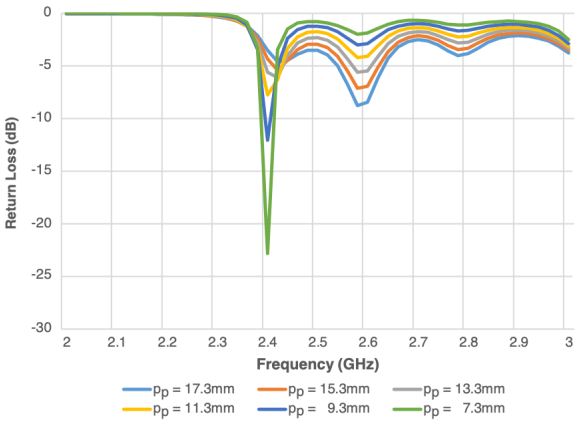

Fig. 6. Return loss at Port #3 as varied port position.

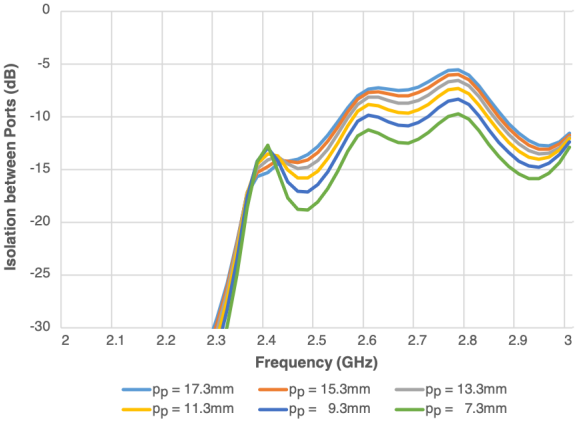

Fig. 7. Isolations between output ports as varied Port #3 position.

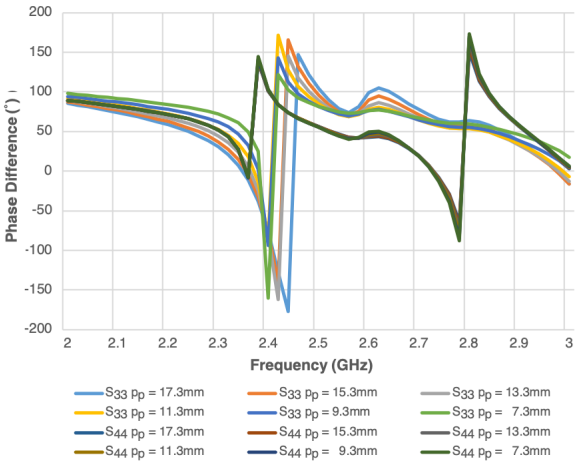

Fig. 8. Phase difference at output port as varied Port #3 position.

D. Variation of Slot Position

The slot involved in the design of SIW-based feeding network plays an essential role to connect the *E*-arm and the *H*-arm through collinear arms. All observed parameters previously aforementioned will be remarkably affected due to the variation

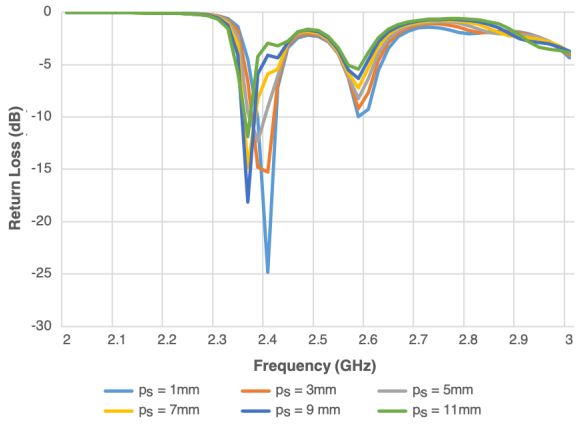

Fig. 9. Return loss at Port #2 as varied slot position.

of slot position, however the most significant occurred on Port #2. The frequency shift at Port #2 and the depth of return loss are very significant changes as shown in Fig. 9. The closer the slot position to Port #2 causes the return loss increases and the working frequency shift decreases away from the desired one the frequency of 2.4 GHz. When the slot position is 1 mm from the edge of *E*-arm, the return loss –24.808 dB is obtained at Port #2. This position is the optimum distance and will be implemented for the fabrication.

III. Characterization Result

The fabrication of proposed SIW-based feeding network is carried out based on the optimum design result previously described. The experimental characterization and measurement are performed using a Vector Network Analyzer whereby the measured results are compared with the simulated ones. The picture of realized SIW-based feeding network is shown in Fig. 10. A 50 Ω SMA connector is attached and soldered on each port. The realized horizontal *E*-arm is then placed above the realized collinear arms and attached using adhesive tape to connect the realized *H*-arm through a slot. Figs. 11 and 12 plot the comparison of measured and simulated return losses at the input and output ports, respectively. The results show

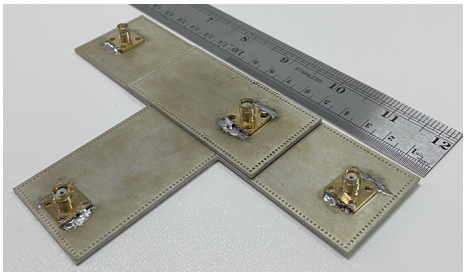

Fig. 10. Picture of realized SIW-based feeding network.

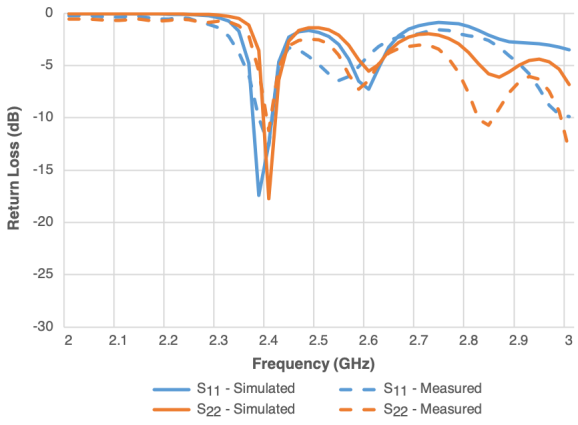

Fig. 11. Measured and simulated return losses at input ports.

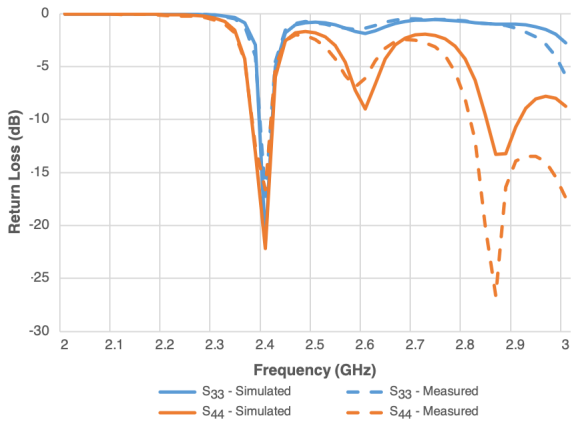

Fig. 12. Measured and simulated return losses at output ports.

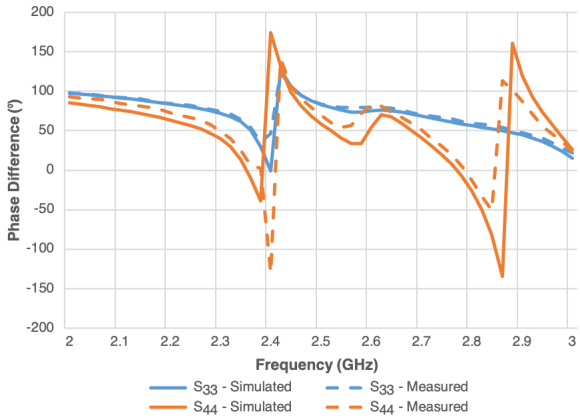

Fig. 13. Measured and simulated phase differences at Port #3 and Port #4.

that measured return losses have good agreement and similar performance compared to the simulated ones for both ports. The working frequency for all ports reaches 2.4 GHz with a slight difference in the depth of return loss.

Fig. 13 depicts the comparison of measured and simulated phase difference between Port #3 and Port #4. It seems that the phase difference for Port #4 at the frequency of 2.4 GHz has a minor variation for both measurement and simulation. Meanwhile, the comparison of measured and simulated insertion loss and isolation shown in Fig. 14 has a similar trend for both characterizations. Some discrepancies occurred between the measured and simulated results are mostly evoked by the manufacturing process, in which some assembly issues affect the slot position when connecting the *E*-arm to the *H*-arm and yield the gaps between the arms. Nevertheless, the performance of realized SIW-based feeding network for S-band monopulse antenna are comparable to the simulated ones, and therefore it is adequate for the desired application in tracking system.

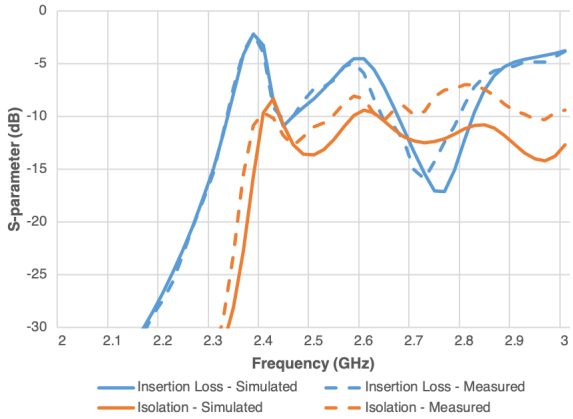

Fig. 14. Measured and simulated insertion losses and isolations.

IV. Conclusion

The design and characterization of SIW-based feeding network for S-band monopulse antenna have been presented. The proposed SIW-based feeding network which consists of a horizontal *E*-plane arm placed above the *H*-plane arm, has a dimension of 158.2 mm × 100.8 mm. The dimensions of *E*-arm and *H*-arm, port and slot positions significantly affected the return loss, isolation, and phase difference. The characterization results have shown that the proposed SIW-based feeding network could produce return loss of less than –10 dB, isolation less than –10 dB, and phase difference around 180°. In addition, the SIW-based feeding network using microstrip line as port excitations will be the future work.

References

[1] H. Chen, W. Che, Q. He, W. Feng, X. Wei, and K. Wu, "Compact substrate integrated waveguide (SIW) monopulse network for *Ku*–band tracking system applications," *IEEE Trans. Microw. Theory Tech.*, vol. 62, no. 3, pp. 472–480, Mar. 2014, DOI: 10.1109/TMTT.2014.2303428.

[2] V. W. Paradkar, R. Saha, K. Sreekumar, and S. B. Sharma, "Horn feed with switchable polarization for radar and tracking antenna system," in *Proc. International Conference on Range Technology (ICORT)*, Balasore, India, Feb. 2019, pp. 1–3, DOI: 10.1109/ICORT46471.2019.9069605.

[3] A. Kurniawan and S. Mukhlishin, "Wideband and multiband antenna design and fabrication for modern wireless communications systems," *J. ICT Res. Appl.*, vol. 7, no. 2, pp. 151–163, Nov. 2013, DOI: 10.5614/itbj.ict.res.appl.2013.7.2.4.

[4] N. D. Tan, L. N. Giang, and N. D. Viet, "Modelling and simulation of a hexapod antenna system for tracking VNREDSAT-1 satellite," in *Proc. IEEE International Conference on Environment and Electrical Engineering and 2020 IEEE Industrial and Commercial Power Systems Europe (EEEIC / I and CPS Europe)*, Madrid, Spain, Jun. 2020, pp. 1–6, DOI: 10.1109/EEEIC/ICPSEurope49358.2020.9160586.

[5] F. Cao, D. Yang, J. Pan, D. Geng, and H. Xiao, "A compact single-layer substrate-integrated waveguide (SIW) monopulse slot antenna array," *IEEE Antennas Wireless Propag. Lett.*, vol. 16, pp. 2755–2758, Aug. 2017, DOI: 10.1109/LAWP.2017.2744668.

[6] E. Novendra, A. Munir, A. B. Rifa'i, and N. Ismail, "Characterization of SIW-based 5.8 GHz monopulse antenna using type-V linear slot," in *Proc. 7th International Conference on Wireless and Telematics (ICWT)*, Bandung, Indonesia, Aug. 2021, pp. 1–4, DOI: 10.1109/ICWT52862.2021.9678199.

[7] B. Wu, R. Tang, Z. Zhou, L. Chen, and T. Zhang, "A double-layer 2-D monopulse SIW slot array antenna using cavity resonators," in *Proc. Cross Strait Radio Science and Wireless Technology Conference (CSRSWTC)*, Shenzhen, China, Oct. 2021, pp. 248–250, DOI: 10.1109/CSRSWTC52801.2021.9631632.

[8] G.-L. Huang, S.-G. Zhou, and T.-H. Chio, "Highly-efficient self-compact monopulse antenna system with integrated comparator network for RF industrial applications," *IEEE Trans. Ind. Electron.*, vol. 64, no. 1, pp. 674–681, Jan. 2017, DOI: 10.1109/TIE.2016.2608769.

[9] S. Peng, Y. Pu, Z. Wu, and Y. Luo, "Compact *Ka*–band magic-T using waveguide to microstrip dual-probe transition," *IEEE Microw. Wireless Compon. Lett.*, vol. 32, no. 8, pp. 946–949, Aug. 2022, DOI: 10.1109/LMWC.2022.3161927.

[10] D. Deslandes and K. Wu, "Accurate modeling, wave mechanisms, and design considerations of a substrate integrated waveguide," *IEEE Trans. Microw. Theory Tech.*, vol. 54, no. 6, pp. 2516–2526, Jun. 2006, DOI: 10.1109/TMTT.2006.875807.

[11] Z. Taha, H. Jassim, A. Ahmed, and I. Farhan, "Design and implementation of triple band half mode substrate integrated waveguide (HMSIW) antenna with compact size," *J. ICT Res. Appl.*, vol. 15, no. 2, pp. 120–138, Oct. 2021, DOI: 10.5614/itbj.ict.res.appl.2021.15.2.2.

[12] D. Nagaraju and Y. K. Verma, "A compact wideband planar magic tee for monopulse antenna array applications," *IEEE Microw. Wireless Compon. Lett.*, vol. 31, no. 5, pp. 429–432, May 2021, DOI: 10.1109/LMWC.2021.3065573.

[13] V. S. Kumar and D. G. Kurup, "A new broadband magic tee design for Ka-band satellite communications," *IEEE Microw. Wireless Compon. Lett.*, vol. 29, no. 2, pp. 92–94, Feb. 2019, DOI: 10.1109/LMWC.2018.2886193.

[14] M. Liu and Z. Feng, "A novel hybrid planar SIW magic Tee," in *Proc. Asia-Pacific Microwave Conference*, Hong Kong, China, Dec. 2008, pp. 1–4, DOI: 10.1109/APMC.2008.4958212.

[15] W. Feng, W. Che, and K. Deng, "Compact planar magic-T using E-plane substrate integrated waveguide (SIW) power divider and slotline transition," *IEEE Microw. Wireless Compon. Lett.*, vol. 20, no. 6, pp. 331–333, Jun. 2010, DOI: 10.1109/LMWC.2010.2047519.

[16] J. Huang, G. Hua, B. Cao, and F. Ran, "A 34.5GHz planar magic-T based on coupling slot and substrate integrated waveguide," in *Proc. IEEE International Conference on Ubiquitous Wireless Broadband (ICUWB)*, Nanjing, China, Oct. 2016, pp. 1–3, DOI: 10.1109/ICUWB.2016.7790482.

[17] P. Wu, S. Liao, and Q. Xue, "A substrate integrated magic-T based on higher order mode cavity and slotline," in *Proc. Asia-Pacific Microwave Conference (APMC)*, Nanjing, China, Dec. 2015, pp. 1–3, DOI: 10.1109/APMC.2015.7413074

[18] L. Yang, F. Xu, S. Deng, and S. Liu, "A compact planar magic-T using quarter-mode substrate integrated waveguide resonator and slotline coupling transition," in *Proc. IEEE International Conference on Ubiquitous Wireless Broadband (ICUWB)*, Nanjing, China, Oct. 2016, pp. 1–3, DOI: 10.1109/ICUWB.2016.7790532.

[19] R. Haro-Baéz, J. P. Burbano-Guerrero, and D. S. Bentez, "On the design of truncated T-type power dividers for X-band with SIW technology," in *Proc. IEEE ANDESCON*, Quito, Ecuador, Oct. 2020, pp. 1–6, DOI: 10.1109/ANDESCON50619.2020.9271978.

[20] A. Izzuddin, A. Dewantari, E. Setijadi, E. Palantei, E. T. Rahardjo, and A. Munir, "Design of 2.4 GHz slotted SIW array antenna for WLAN application," in *Proc. International Conference on Radar, Antenna, Microwave, Electronics, and Telecommunications (ICRAMET)*, Tangerang, Indonesia, Nov. 2020, pp. 70–73, DOI: 10.1109/ICRAMET51080.2020.9298646.